Quantized Spin Pumping in Topological Ferromagnetic-Superconducting Nanowires

V. Fernández Becerra,[1,*] Mircea Trif,[1] and Timo Hyart[1,2,3]

[1]*International Research Centre MagTop, Institute of Physics, Polish Academy of Sciences, Aleja Lotnikow 32/46, PL-02668 Warsaw, Poland*

[2]*Department of Applied Physics, Aalto University, 00076 Aalto, Espoo, Finland*

[3]*Computational Physics Laboratory, Physics Unit, Faculty of Engineering and Natural Sciences, Tampere University, FI-33014 Tampere, Finland*

(Received 14 June 2022; revised 20 April 2023; accepted 16 May 2023; published 7 June 2023)

Semiconducting nanowires with strong spin-orbit coupling in the presence of induced superconductivity and ferromagnetism can support Majorana zero modes. We study the pumping due to the precession of the magnetization in single-subband nanowires and show that spin pumping is robustly quantized when the hybrid nanowire is in the topologically nontrivial phase, whereas charge pumping is not quantized. Moreover, there exists one-to-one correspondence between the quantized conductance, entropy change and spin pumping in long topologically nontrivial nanowires but these observables are uncorrelated in the case of accidental zero-energy Andreev bound states in the trivial phase. Thus, we conclude that observation of correlated and quantized peaks in the conductance, entropy change and spin pumping would provide strong evidence of Majorana zero modes, and we elaborate how topological Majorana zero modes can be distinguished from quasi-Majorana modes potentially created by a smooth tunnel barrier at the lead-nanowire interface. Finally, we discuss peculiar interference effects affecting the spin pumping in short nanowires at very low energies.

DOI: 10.1103/PhysRevLett.130.237002

Introduction.—One of the most challenging aims in the current condensed matter physics research is the demonstration of non-Abelian Majorana statistics—the underlying fundamental property that would enable the realization of a topological quantum computer [1–5]. It is theoretically well established that Majorana zero modes (MZMs) can be realized in semiconducting nanowires with strong Rashba spin-orbit coupling in the presence of induced superconductivity and external magnetic field [6,7]. One of the hallmark features of the MZMs is the resonant Andreev reflection, which gives rise to a quantized zero-bias peak in the conductance [8,9]. Although zero-bias conductance peaks have been observed in experiments [10], it is known that formation of unwanted quantum dots or unintentional inhomogeneities at the lead-nanowire interface can lead to non-Majorana zero-bias conductance peaks [11–20], and therefore the current attempts to demonstrate the existence of MZMs utilize multimodal experimental data with sophisticated protocols to reduce the likelihood of false positives [21,22]. Other techniques to detect MZMs based on noise [23–26] and entropy change [27–30] are also being developed.

The advent of hybrid ferromagnetic insulator-superconducting (FI-SC) nanowire devices [31,32] opens paths for novel approaches for probing the existence of MZMs. In this Letter, we study the charge and spin pumping in this system in the presence of precessing magnetization. The precessing magnetization is a well-established method for generating spin current in magnetic heterostructures and forms the basis of many contemporary spintronics applications [33–38]. It is known that under some specific circumstances the precessing magnetization can also lead to quantized charge and spin pumping [39–43], which can be understood as Thouless pumping in the Hamiltonian formalism [44] and topological winding number in the scattering matrix formalism [43]. Here, we apply the scattering matrix formalism to the case of FI-SC nanowire devices, and find an unprecedented case where the charge pumping is nonquantized, in agreement with the previous study [45], but the spin pumping is robustly quantized. We show that in long single-subband nanowires there exists one-to-one correspondence between the quantized conductance, entropy change, and the quantized spin pumping in the topologically nontrivial nanowires, but these observables are uncorrelated in the case of accidental zero-energy Andreev bound states in the trivial phase. Thus, we conclude that the observation of correlated and quantized peaks in the conductance, entropy change, and spin pumping would provide strong evidence of MZMs, and we elaborate how topological MZMs can be distinguished from quasi-Majorana modes potentially created by imperfections at the lead-nanowire interface. Furthermore, we identify a suitable regime of system parameters for observing the quantization and consider interference effects in short nanowires, which affect the conductance and spin pumping differently at very low energies. Finally, we show that the quantized spin pumping can be detected from the absorption linewidth of the precessing FI.

Spin and charge pumping in long nanowires.—We consider the system shown in Fig. 1(a) described by a Bogoliubov–de Gennes (BdG) Hamiltonian

$$\mathcal{H}(t) = \left[\frac{p^2}{2m} - \alpha_R p \sigma_z - \mu(x)\right]\tau_z + \boldsymbol{m}(x,t)\cdot\boldsymbol{\sigma} + \Delta(x)\tau_x, \tag{1}$$

where $\boldsymbol{\sigma} = (\sigma_x, \sigma_y, \sigma_z)$ and $\boldsymbol{\tau} = (\tau_x, \tau_y, \tau_z)$ are Pauli matrices that act in the spin and Nambu space, respectively, $p = -i\hbar\partial_x$ is the momentum operator along the wire (x-direction), m is the effective electron mass, α_R is the Rashba spin-orbit coupling strength, $\boldsymbol{m}(x,t) = m_0\Theta(x)[\sin\theta\cos\phi(t), \sin\theta\sin\phi(t), \cos\theta]$ is the magnetic exchange field induced by the precessing magnetization of a ferromagnetic insulator, $\Delta(x) = \Delta_0\Theta(x)$ is the induced superconducting order parameter, $\Theta(x)$ is the Heaviside step function, and $\mu(x)$ is the chemical potential. We denote the chemical potentials in the lead, tunnel barrier and FI-SC nanowire as μ_N, $\mu_{\rm tun}$, and μ, respectively. We consider periodic driving $\boldsymbol{m}(x, t+\mathcal{T}) = \boldsymbol{m}(x,t)$ with period $\mathcal{T} = 2\pi/\omega$ and frequency ω, and measure energies, momenta, and lengths in units of $E_{\rm SO} = m\alpha_R^2/2$, $p_{\rm SO} = 2m\alpha_R$ and $\ell_{\rm SO} = \hbar/p_{\rm SO}$, respectively. The phase diagram of this system is shown in Fig. 1(b). The gapped phases of FI-SC nanowires are classified by the one-dimensional class D $\mathbb{Z}_2$ topological invariant which determines the existence of topologically protected MZMs at the end of the wire [46]. The topologically nontrivial gapped phase emerges in the regime $\sqrt{\Delta_0^2+\mu^2} < m_0 < \Delta_0/\cos\theta$ and the system is gapless if $m_0 > \Delta_0/\cos\theta$. In the following we stay in the parameter regime where the FI-SC nanowire is gapped. The width of the tunnel barrier is $4\ell_{\rm SO}$ and $\mu_N = 0$. For other barrier widths see Ref. [47].

The precessing magnetization pumps charge and spin from the FI-SC nanowire into the lead. The pumped charge Q and spin S_z over one cycle in the adiabatic limit can be calculated from the expression [53,54]

$$\mathcal{O} = \int dE\left(\frac{\partial f}{\partial E}\right)\int_0^{\mathcal{T}} dt\, \mathrm{Im}\left\{\mathrm{Tr}\left[\hat{r}^\dagger\hat{\mathcal{O}}\frac{\partial\hat{r}}{\partial t}\right]\right\}, \tag{2}$$

where $f(E)$ is the Fermi function, the operator $\hat{\mathcal{O}}$ for the pumped charge (spin) is $\hat{Q} = e\tau_z/4\pi$ ($\hat{S}_z = \hbar\sigma_z/8\pi$), and $\hat{r}[E,\phi(t)]$ is the instantaneous scattering matrix

$$\hat{r} = \begin{pmatrix} \hat{r}_{ee} & \hat{r}_{eh} \\ \hat{r}_{he} & \hat{r}_{hh}\end{pmatrix}, \qquad \hat{r}_{ee} = \begin{pmatrix} r_{ee}^{\uparrow\uparrow} & r_{ee}^{\uparrow\downarrow} \\ r_{ee}^{\downarrow\uparrow} & r_{ee}^{\downarrow\downarrow}\end{pmatrix},$$

$$\hat{r}_{he} = \begin{pmatrix} r_{he}^{\downarrow\uparrow} & r_{he}^{\downarrow\downarrow} \\ r_{he}^{\uparrow\uparrow} & r_{he}^{\uparrow\downarrow}\end{pmatrix}$$

accounting for the normal $\hat{r}_{ee}$ and Andreev $\hat{r}_{he}$ processes. The other blocks can be obtained via particle-hole symmetry $\tau_y\sigma_y\hat{r}^*(-E)\tau_y\sigma_y = \hat{r}(E)$. In a continuous operation of the device the time averages of the pumped charge and spin currents can be written, respectively, as $\langle I_e\rangle = \omega Q/2\pi$ and $\langle I_s\rangle = \omega S_z/2\pi$.

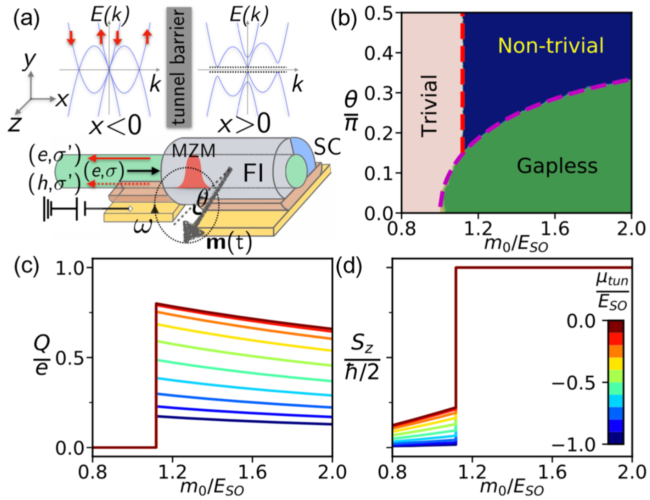

FIG. 1. (a) Rashba nanowire (green) with proximity induced superconductivity (blue) and magnetization (gray) supports MZM (red). The tunnel barrier $\mu_{\rm tun}$ can be controlled with a gate voltage. The precessing magnetization $\boldsymbol{m}(t)$ pumps spin and charge into the lead ($x<0$) due to the normal and Andreev reflection processes. (b) Topological phase diagram of the FI-SC nanowire as a function of m_0 and θ. The phase transition line separating the gapped phases is given by $\Delta_0^2+\mu^2 = m_0^2$ and the transition between gapped and gapless phase occurs at $\Delta_0 = m_0\cos\theta$. (c),(d) The pumped charge Q and spin S_z as a function of m_0 for different $\mu_{\rm tun}$. The pumped spin is quantized to $S_z = \hbar/2$ in the topologically nontrivial regime. The results have been calculated for $\Delta_0 = E_{\rm SO}$, $\mu = 0.5E_{\rm SO}$, and $\theta = 2\pi/5$ in the limit k_BT, $\omega\to 0$.

In the case of uniform precession (or arbitrary adiabatic precession) the time dependence of the Hamiltonian can be removed by switching to the rotating frame $\mathcal{H}_{\rm rot} = U^\dagger\mathcal{H}_{BdG}(t)U - i\hbar U^\dagger\partial_t U$ via unitary transformation $U = e^{-i\phi(t)\sigma_z/2}$. The coefficients $\tilde{r}_{ee}^{\sigma\sigma'}$ and $\tilde{r}_{he}^{\sigma\sigma'}$ can then be obtained by finding a solution $\Psi_{\rm rot}(x)$ of the time-independent Hamiltonian $\mathcal{H}_{\rm rot}$, and the scattering states in the lab frame are obtained using $\Psi(x,t) = U\Psi_{\rm rot}(x)$. This way we find that the only t-dependent reflection coefficients are

$$r_{ee}^{\bar{\beta}\beta}(t) = \tilde{r}_{ee}^{\bar{\beta}\beta}e^{i\beta\phi(t)}, \qquad r_{he}^{\beta\beta}(t) = \tilde{r}_{he}^{\beta\beta}e^{i\beta\phi(t)},$$

where $\bar{\beta} = -\beta$, and we use $\beta = +1, -1$ and $\uparrow, \downarrow$ interchangeably. Using these expressions we obtain

$$Q = \int dE\left(-\frac{\partial f}{\partial E}\right)\mathcal{Q}(E),$$

$$S_z = \int dE\left(-\frac{\partial f}{\partial E}\right)\mathcal{S}_z(E),$$

$$\mathcal{Q}(E) = e(|r_{ee}^{\uparrow\downarrow}|^2 - |r_{ee}^{\downarrow\uparrow}|^2 + |r_{he}^{\uparrow\uparrow}|^2 - |r_{he}^{\downarrow\downarrow}|^2),$$

$$\mathcal{S}_z(E) = \hbar(|r_{ee}^{\uparrow\downarrow}|^2 + |r_{ee}^{\downarrow\uparrow}|^2 + |r_{he}^{\uparrow\uparrow}|^2 + |r_{he}^{\downarrow\downarrow}|^2)/2. \tag{3}$$

In the limit of low temperature $k_B T \to 0$ and frequency $\omega \to 0$ the pumped charge (spin) is related to the corresponding spectral density as $Q = \mathcal{Q}(0)$ $[S_z = \mathcal{S}_z(0)]$. These formulas can be generalized to arbitrary ω by evaluating the contributions of the scattering paths in the rotating frame taking into account the spin bias terms in the distribution functions as described in Ref. [43]. The general expression is obtained from Eq. (3) by replacing $\partial f/\partial E$ with a "quantum derivative" $[f(E + \hbar\omega/2) - f(E - \hbar\omega/2)]/\hbar\omega$ and computing the reflection coefficients in the presence of the term $-i\hbar U^\dagger \partial_t U = -\hbar\omega\sigma_z/2$. In the absence of a bias voltage the spectral densities are weighted with symmetric functions in the energy integrals. Hence, in some figures it is more illustrative to plot the symmetrized spectral density $\mathcal{S}_z^s(E) = [\mathcal{S}_z(E) + \mathcal{S}_z(-E)]/2$.

Figures 1(c) and 1(d) show representative results for Q and S_z obtained by numerically calculating the reflection matrix for long FI-SC nanowires using Kwant software package [55]. Both quantities take arbitrary (typically small) values in the case of topologically trivial wires. By tuning the parameters of the system to the topologically nontrivial phase we observe a sharp transition in Q and S_z. Within the topologically nontrivial phase Q still takes arbitrary values depending on the m_0, θ and tunnel barrier $\mu_{\rm tun}$ introduced between the lead and the system, similarly as obtained in the previous studies [45]. On the other hand, S_z is now robustly quantized to $\hbar/2$ at low temperatures and frequencies.

Correspondence of spin pumping, conductance, and entropy.—One of the hallmarks of the nontrivial topology is the robust quantization of the differential conductance

$$G = \int dE \left(-\frac{\partial f}{\partial E}\right) \mathcal{G}(E), \qquad \mathcal{G}(E) = 2G_0 \mathrm{Tr}[\hat{r}_{he}^\dagger \hat{r}_{he}] \quad (4)$$

to a universal value $G = 2G_0$ ($G_0 = e^2/h$) at small bias voltages in the tunneling regime [8]. Moreover, in ballistic point contacts this zero-bias peak widens into a plateau of quantized conductance [9]. We show that in long nanowires there exists one-to-one correspondence between the quantization of the conductance $G = 2G_0$ and the spin pumping $S_z = \hbar/2$ in the nontrivial regime. For this purpose we consider the scattering states in the lead [$x < 0$ in Fig. 1(a)] at energy $E = 0$ and $\omega \to 0$

$$\Psi_{\rm rot}^{\alpha,L}(x) = \begin{pmatrix} \chi_\alpha \\ 0 \end{pmatrix} e^{ixk_{\rm in}^\alpha} + \sum_\beta \left[\tilde{r}_{ee}^{\beta\alpha} \begin{pmatrix} \chi_\beta \\ 0 \end{pmatrix} e^{-ixk_o^\beta} + \tilde{r}_{he}^{\beta\alpha} \begin{pmatrix} 0 \\ \chi_{\bar{\beta}} \end{pmatrix} e^{ixk_o^\beta} \right],$$

composed of an incoming electron with spin-z eigenvalue $\alpha = \pm 1$ in eigenstate $\chi_\alpha = (1+\alpha, 1-\alpha)^T/2$ and $k_{\rm in}^\alpha \ell_{\rm SO} = (\alpha + \sqrt{1 + \mu_N/E_{\rm SO}})/2$, and four outgoing states with $k_o^\beta \ell_{\rm SO} = (-\beta + \sqrt{1 + \mu_N/E_{\rm SO}})/2$. The reflection coefficients $\tilde{r}_{ee}^{\beta\alpha}$ and $\tilde{r}_{he}^{\beta\alpha}$ are obtained by matching the

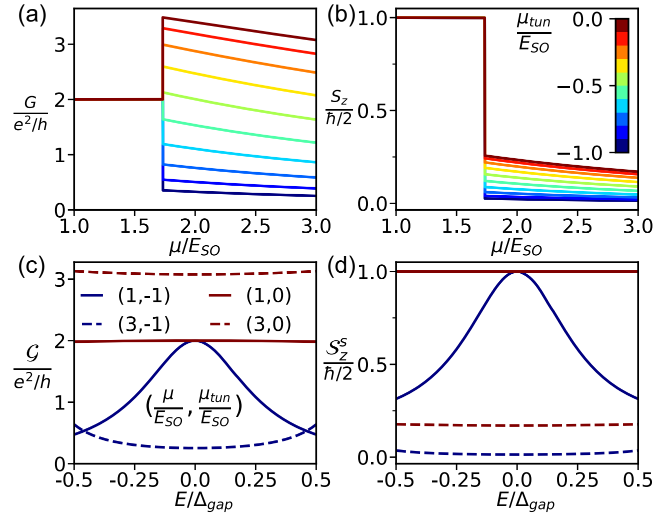

FIG. 2. (a) G and (b) S_z as a function of μ for different $\mu_{\rm tun}$ in the limit $\omega, k_B T \to 0$. In the topologically nontrivial phase ($\mu < \sqrt{3}E_{\rm SO}$) there is a perfect correspondence between the quantized conductance $G = 2G_0$ and spin pumping $S_z = \hbar/2$, but these observables are unrelated in the trivial regime ($\mu > \sqrt{3}E_{\rm SO}$). (c),(d) The spectral densities $\mathcal{G}(E)$ and $\mathcal{S}_z^s(E)$ in the nontrivial ($\mu = E_{\rm SO}$) and trivial ($\mu = 3E_{\rm SO}$) phases in the tunneling regime $\mu_{\rm tun} = -E_{\rm SO}$ and in the absence of tunnel barrier $\mu_{\rm tun} = 0$. The energy is normalized with the gap $\Delta_{\rm gap}$ in the FI-SC nanowire. The model parameters are $\Delta_0 = E_{\rm SO}$, $m_0 = 2E_{\rm SO}$, and $\theta = 2\pi/5$.

solutions $\Psi_{\rm rot}^{\alpha,L}(0) = \Psi_{\rm rot}^{\alpha,R}(0)$ and $\partial_x \Psi_{\rm rot}^{\alpha,L}(0) = \partial_x \Psi_{\rm rot}^{\alpha,R}(0)$, where $\Psi_{\rm rot}^{\alpha,R}(x)$ are the evanescent states in the FI-SC nanowire [$x > 0$ in Fig. 1(a)]. This way we arrive at the following expressions [47]

$$|\tilde{r}_{ee}^{\beta\beta}| = \frac{|k_o^{\bar{\beta}} - iz_4||k_o^\beta - iz_4|}{\sum_\sigma (k_o^\sigma)^2 + 2z_4^2}, \qquad |\tilde{r}_{ee}^{\bar{\beta}\beta}| = \frac{(k_o^\beta)^2 + z_4^2}{\sum_\sigma (k_o^\sigma)^2 + 2z_4^2},$$

$$|\tilde{r}_{he}^{\bar{\beta}\beta}| = \frac{(k_o^{\bar{\beta}})^2 + z_4^2}{\sum_\sigma (k_o^\sigma)^2 + 2z_4^2}, \qquad |\tilde{r}_{he}^{\beta\beta}| = \frac{|k_o^{\bar{\beta}} + iz_4||k_o^\beta - iz_4|}{\sum_\sigma (k_o^\sigma)^2 + 2z_4^2},$$

where z_4 is the only root of the quartic polynomial

$$\left(4z_4^2 \ell_{\rm SO}^2 + \frac{\mu}{E_{\rm SO}}\right)^2 + \left(4z_4 \ell_{\rm SO} - \frac{\Delta_e}{E_{\rm SO}}\right)^2 - \frac{m_0^2 \sin^2\theta}{E_{\rm SO}^2} = 0,$$

having $\Re[z_4] > 0$ (evanescent mode). Thus, $z_4 \in \mathbb{R}$. Here, $\Delta_e = \sqrt{\Delta_0^2 - m_0^2 \cos^2\theta} > 0$ in the gapped phase. Because $|r_{ee}^{\beta\beta}| = |r_{he}^{\beta\beta}|$, it follows from Eqs. (3) and (4) that

$$\frac{\mathcal{S}_z(0)}{\hbar/2} = \mathrm{Tr}[\hat{r}_{ee}^\dagger \hat{r}_{ee}] = 2 - \mathrm{Tr}[\hat{r}_{he}^\dagger \hat{r}_{he}] = 2 - \frac{\mathcal{G}(0)}{2G_0}. \quad (5)$$

Therefore, in long nanowires there is a perfect correspondence between the quantized spin pumping $\mathcal{S}_z(0) = \hbar/2$ and the quantized conductance $\mathcal{G}(0) = 2G_0$ in the topologically nontrivial regime. This correspondence is illustrated in Fig. 2. In the tunneling regime there exists quantized peaks in $\mathcal{S}_z^s(E)$ and $\mathcal{G}(E)$ at $E = 0$, which widen

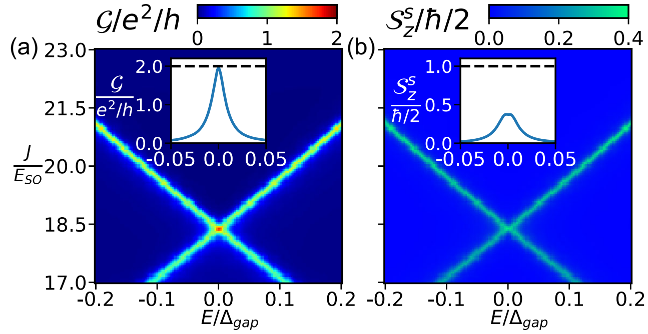

FIG. 3. The impurity induced Andreev bound states crossing zero energy give rise to peaks in (a) $\mathcal{G}(E)$ and (b) $\mathcal{S}_z^s(E)$ at $E = 0$. The heights of the peaks are arbitrary but they can accidentally have a quantized value as shown in (a). However, the heights of the peaks in $\mathcal{G}(E)$ and $\mathcal{S}_z^s(E)$ are unrelated to each other. Therefore, accidental low-energy Andreev bound states can be distinguished from the MZMs, which give rise to correlated quantized peaks in $\mathcal{G}(E)$ and $\mathcal{S}_z^s(E)$ at $E = 0$ (cf. Fig. 2). Here the impurity states have been induced with a magnetic impurity $J\sigma_z$ located at the lattice site $x_i = 6\ell_{\rm SO}$. The model parameters are $\Delta_0 = E_{\rm SO}$, $\mu = 0$, $m_0 = 0.3E_{\rm SO}$, $\theta = \pi/2$, $\mu_{\rm tun} = -1.5E_{\rm SO}$ and lattice constant $d = \ell_{\rm SO}/4$.

into plateaus upon decreasing the tunnel barrier to $\mu_{\rm tun} = 0$. Importantly, $\mathcal{S}_z^s(E)$ and $\mathcal{G}(E)$ are unrelated to each other in the topologically trivial nanowires. We find that similar correlation exists also between quantized entropy change and spin pumping in nontrivial wires [47].

Distinguishing MZMs from Andreev bound states and quasi-MZMs.—The combined measurements of the spin pumping and conductance could also be helpful in distinguishing non-Majorana zero-bias conductance peaks [11–20] from the zero-bias peaks caused by the MZMs. To demonstrate this, we have computed the effect of non-Majorana Andreev bound states, induced by a magnetic impurity pointing along the spin z direction, on the conductance and spin pumping in the trivial regime (see Fig. 3). The impurity induced Andreev bound states can give rise to zero-energy peaks in $\mathcal{G}(E)$ and $\mathcal{S}_z^s(E)$. The heights of the peaks are arbitrary but they can accidentally have a quantized value. However, the heights of the peaks in $\mathcal{G}(E)$ and $\mathcal{S}_z^s(E)$ are unrelated to each other. Therefore accidental low-energy Andreev bound states can be distinguished from the MZMs, which give rise to correlated quantized peaks in $\mathcal{G}(E)$ and $\mathcal{S}_z^s(E)$ at $E = 0$ (cf. Figs. 2 and 3). We point out that a smooth tunnel barrier can induce two spatially separated MZMs at the lead-nanowire interface [11–15,17], and in certain cases these quasi-MZMs are so weakly coupled to each other that they can mimic all properties of the MZMs, including quantized conductance, 4π Josephson effect and even the non-Abelian braiding statistics [17,56]. However, the quantized spin pumping and conductance are independent of the strength of the tunnel barrier, and therefore the topological MZMs can be distinguished from quasi-MZMs by demonstrating the robustness

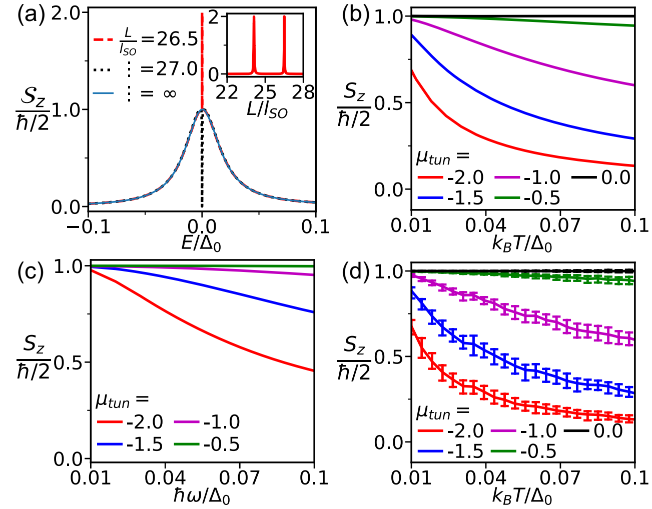

FIG. 4. (a) The dependence of $\mathcal{S}_z(E)$ on the length L of the wire. The hybridization of the MZMs and the interference effects lead to appearance of a very sharp peak or a dip at very low energies. (b) S_z as a function of k_BT for $\omega \to 0$. (c) S_z as a function of ω for $k_BT \to 0$. (d) S_z as a function of k_BT for $\omega \to 0$ in the presence of disorder potential $V(x)\tau_z$, where the $V(x)$ at each lattice site x are uncorrelated uniformly distributed random numbers between $[-8E_{\rm SO}, 8E_{\rm SO}]$ and we have used lattice constant $d = \ell_{\rm SO}/50$. The error bars denote the 10th and 90th percentile values. The model parameters are $\Delta_0 = E_{\rm SO}$, $\mu = 0$, $m_0 = 2E_{\rm SO}$, and $\theta = \pi/2$. In (a) $\mu_{\rm tun} = -2E_{\rm SO}$, in (b),(c) and (d) $L = 26.5\ell_{\rm SO}$.

of the quantized signatures upon lowering of the tunnel barrier [47].

Parametric dependencies.—The dependence of $\mathcal{S}_z(E)$ on the length L of the FI-SC wire is shown in Fig. 4(a), where $m(x) = m_0\Theta(L - x)\Theta(x)$. The overall shape is similar to the case of $L \to \infty$, but the hybridization of the MZMs and the interference effects lead to a very sharp dip or a peak at very low energies. Their widths decrease exponentially with L so that robust quantization of S_z exists at experimentally relevant temperatures and frequencies if L is sufficiently large and the tunnel barrier is not too large [Figs. 4(b) and 4(c)]. The quantization of S_z is robust in the presence of disorder [Fig. 4(d)], but very strong disorder leads to large sample-to-sample fluctuations of S_z at very small temperatures and frequencies due to the sharp peaks and dips in $\mathcal{S}_z(E)$ [47].

We can capture the essential physics behind the shape of the $\mathcal{S}_z(E)$ using the Mahaux-Weidenmüller formula for the scattering matrix [57–59]

$$S = 1 - 2\pi i W^\dagger (E - H_M + i\pi W W^\dagger)^{-1} W,$$

$$H_M = i\begin{pmatrix} 0 & E_M \\ -E_M & 0 \end{pmatrix}, \qquad W = \begin{pmatrix} w_\uparrow^L & w_\downarrow^L & w_\uparrow^{L*} & w_\downarrow^{L*} \\ w_\uparrow^R & w_\downarrow^R & w_\uparrow^{R*} & w_\downarrow^{R*} \end{pmatrix}, \quad (6)$$

where H_M describes the coupling E_M between the left and right MZMs and W the coupling of MZMs to the lead modes in the basis $(c_\uparrow^\dagger, c_\downarrow^\dagger, -c_\uparrow, -c_\downarrow)$. Without loss of generality we can choose $0 < w_\uparrow^L, w_\downarrow^L \in \mathbb{R}$. Moreover, the couplings of the lead modes to the left MZM w_σ^L are always much larger than the couplings to the right MZM w_σ^R. By neglecting the corrections caused by w_σ^R we obtain $\mathcal{G}(E)/(2G_0) = \mathcal{S}_z(E)/(\hbar/2) = \mathcal{F}(E)$ [47], where

$$\mathcal{F}(E) = \frac{E^2}{E^2 + (E_M^2 - E^2)^2/\Gamma^2}, \qquad \frac{\Gamma}{2\pi} = \sum_\sigma (w_\sigma^L)^2. \quad (7)$$

This formula accurately describes the shape of the sharp dips typically occurring in the $\mathcal{S}_z(E)$, whereas the peaks originate from the interference effects when E_M is small and the couplings w_σ^R become relevant [47]. Our results agree with the earlier reported dips in $\mathcal{G}(E)$ due to the coupling of MZMs [60], but interestingly the interference effects can turn the dips also into peaks in $\mathcal{S}_z(E)$.

Finally, we note that the out-of-equilibrium electrons act back on the magnet, affecting its dynamics. In particular, the spin current ejected into the leads increases the Gilbert damping parameter $\tilde{\alpha}$ entering in the Landau-Lifshitz-Gilbert equation that describes the magnetization dynamics [35]. We find that in our setup the change in the Gilbert damping is $\Delta\tilde{\alpha} \propto S_z/\sin^2\theta$, which could be used to extract experimentally the pumped spin S_z from ferromagnetic resonance measurements [47]. Alternatively, it could be possible to fabricate nanostructures where the pumped spin current could be measured by utilizing the inverse spin Hall effect [61,62].

Conclusions.—We have shown that spin pumping is robustly quantized and there exists one-to-one correspondence to the quantized conductance and the entropy change in topologically nontrivial nanowires, so that the observation of correlated and quantized peaks in the conductance, entropy change, and spin pumping would provide strong evidence of topological superconductivity. In the adiabatic limit our results can be generalized to arbitrary trajectory in $[\theta(t), \phi(t)]$ space as long as the system stays gapped and topologically nontrivial, and the azimuthal angle $\phi(t)$ winds around the z axis. We have neglected the non-equilibrium effects such as the dynamical spin accumulation at the interface of the FI-SC nanowire and the normal lead. Such effects can lead to nonlinear corrections to the calculated spin current as a function of ω but they do not affect the quantized response at low frequencies where the spin current is proportional to ω. The maximum frequency is limited by the topological energy gap, so we estimate that $\omega \lesssim 10$ GHz [22].

The work is supported by the Foundation for Polish Science through the IRA Programme co-financed by EU within SG OP and the Academy of Finland Project No. 331094. We acknowledge the computational resources provided by the Aalto Science-IT project and the access to the computing facilities of the Interdisciplinary Centre for Mathematical and Computational Modelling (ICM), University of Warsaw, under Grant No. G89-1264.

*victor_f_becerra@outlook.com

[1] C. Nayak, S. H. Simon, A. Stern, M. Freedman, and S. Das Sarma, Non-Abelian anyons and topological quantum computation, Rev. Mod. Phys. **80**, 1083 (2008).

[2] T. Hyart, B. van Heck, I. C. Fulga, M. Burrello, A. R. Akhmerov, and C. W. J. Beenakker, Flux-controlled quantum computation with Majorana fermions, Phys. Rev. B **88**, 035121 (2013).

[3] D. Aasen, M. Hell, R. V. Mishmash, A. Higginbotham, J. Danon, M. Leijnse, T. S. Jespersen, J. A. Folk, C. M. Marcus, K. Flensberg, and J. Alicea, Milestones Toward Majorana-Based Quantum Computing, Phys. Rev. X **6**, 031016 (2016).

[4] T. Karzig, C. Knapp, R. M. Lutchyn, P. Bonderson, M. B. Hastings, C. Nayak, J. Alicea, K. Flensberg, S. Plugge, Y. Oreg, C. M. Marcus, and M. H. Freedman, Scalable designs for quasiparticle-poisoning-protected topological quantum computation with Majorana zero modes, Phys. Rev. B **95**, 235305 (2017).

[5] C. W. J. Beenakker, Search for non-Abelian Majorana braiding statistics in superconductors, SciPost Phys. Lect. Notes 15 (2020), 10.21468/SciPostPhysLectNotes.15.

[6] R. M. Lutchyn, J. D. Sau, and S. Das Sarma, Majorana Fermions and a Topological Phase Transition in Semiconductor-Superconductor Heterostructures, Phys. Rev. Lett. **105**, 077001 (2010).

[7] Y. Oreg, G. Refael, and F. von Oppen, Helical Liquids and Majorana Bound States in Quantum Wires, Phys. Rev. Lett. **105**, 177002 (2010).

[8] K. T. Law, P. A. Lee, and T. K. Ng, Majorana Fermion Induced Resonant Andreev Reflection, Phys. Rev. Lett. **103**, 237001 (2009).

[9] M. Wimmer, A. R. Akhmerov, J. P. Dahlhaus, and C. W. J. Beenakker, Quantum point contact as a probe of a topological superconductor, New J. Phys. **13**, 053016 (2011).

[10] V. Mourik, K. Zuo, S. M. Frolov, S. R. Plissard, E. P. A. M. Bakkers, and L. P. Kouwenhoven, Signatures of Majorana fermions in hybrid superconductor-semiconductor nanowire devices, Science **336**, 1003 (2012).

[11] G. Kells, D. Meidan, and P. W. Brouwer, Near-zero-energy end states in topologically trivial spin-orbit coupled superconducting nanowires with a smooth confinement, Phys. Rev. B **86**, 100503(R) (2012).

[12] C.-X. Liu, J. D. Sau, T. D. Stanescu, and S. Das Sarma, Andreev bound states versus Majorana bound states in quantum dot-nanowire-superconductor hybrid structures: Trivial versus topological zero-bias conductance peaks, Phys. Rev. B **96**, 075161 (2017).

[13] C. Moore, T. D. Stanescu, and S. Tewari, Two-terminal charge tunneling: Disentangling Majorana zero modes from partially separated Andreev bound states in semiconductor-superconductor heterostructures, Phys. Rev. B **97**, 165302 (2018).

[14] C. Moore, C. Zeng, T. D. Stanescu, and S. Tewari, Quantized zero-bias conductance plateau in semiconductor-superconductor heterostructures without topological Majorana zero modes, Phys. Rev. B **98**, 155314 (2018).
[15] B. D. Woods, T. D. Stanescu, and S. Das Sarma, Effective theory approach to the Schrödinger-Poisson problem in semiconductor Majorana devices, Phys. Rev. B **98**, 035428 (2018).
[16] J. Chen, B. D. Woods, P. Yu, M. Hocevar, D. Car, S. R. Plissard, E. P. A. M. Bakkers, T. D. Stanescu, and S. M. Frolov, Ubiquitous Non-Majorana Zero-Bias Conductance Peaks in Nanowire Devices, Phys. Rev. Lett. **123**, 107703 (2019).
[17] A. Vuik, B. Nijholt, A. R. Akhmerov, and M. Wimmer, Reproducing topological properties with quasi-Majorana states, SciPost Phys. **7**, 061 (2019).
[18] E. Prada, P. San-Jose, M. W. A. de Moor, A. Geresdi, E. J. H. Lee, J. Klinovaja, D. Loss, J. Nygård, R. Aguado, and L. P. Kouwenhoven, From Andreev to Majorana bound states in hybrid superconductor–semiconductor nanowires, Nat. Rev. Phys. **2**, 575 (2020).
[19] P. Yu, J. Chen, M. Gomanko, G. Badawy, E. P. A. M. Bakkers, K. Zuo, V. Mourik, and S. M. Frolov, Non-Majorana states yield nearly quantized conductance in proximatized nanowires, Nat. Phys. **17**, 482 (2021).
[20] M. Valentini, F. Peñaranda, A. Hofmann, M. Brauns, R. Hauschild, P. Krogstrup, P. San-Jose, E. Prada, R. Aguado, and G. Katsaros, Nontopological zero-bias peaks in full-shell nanowires induced by flux-tunable Andreev states, Science **373**, 82 (2021).
[21] D. I. Pikulin, B. van Heck, T. Karzig, E. A. Martinez, B. Nijholt, T. Laeven, G. W. Winkler, J. D. Watson, S. Heedt, M. Temurhan, V. Svidenko, R. M. Lutchyn, M. Thomas, G. de Lange, L. Casparis, and C. Nayak, Protocol to identify a topological superconducting phase in a three-terminal device, arXiv:2103.12217.
[22] M. Aghaee *et al.*, InAs-Al hybrid devices passing the topological gap protocol, arXiv:2207.02472.
[23] D. E. Liu, M. Cheng, and R. M. Lutchyn, Probing Majorana physics in quantum-dot shot-noise experiments, Phys. Rev. B **91**, 081405(R) (2015).
[24] D. E. Liu, A. Levchenko, and R. M. Lutchyn, Majorana zero modes choose Euler numbers as revealed by full counting statistics, Phys. Rev. B **92**, 205422 (2015).
[25] S. Smirnov, Majorana finite-frequency nonequilibrium quantum noise, Phys. Rev. B **99**, 165427 (2019).
[26] S. Smirnov, Revealing universal Majorana fractionalization using differential shot noise and conductance in nonequilibrium states controlled by tunneling phases, Phys. Rev. B **105**, 205430 (2022).
[27] S. Smirnov, Majorana tunneling entropy, Phys. Rev. B **92**, 195312 (2015).
[28] E. Sela, Y. Oreg, S. Plugge, N. Hartman, S. Lüscher, and J. Folk, Detecting the Universal Fractional Entropy of Majorana Zero Modes, Phys. Rev. Lett. **123**, 147702 (2019).
[29] S. Smirnov, Majorana entropy revival via tunneling phases, Phys. Rev. B **103**, 075440 (2021).
[30] S. Smirnov, Majorana ensembles with fractional entropy and conductance in nanoscopic systems, Phys. Rev. B **104**, 205406 (2021).
[31] Y. Liu, S. Vaitiekėnas, S. Martí-Sánchez, C. Koch, S. Hart, Z. Cui, T. Kanne, S. A. Khan, R. Tanta, S. Upadhyay, M. E. Cachaza, C. M. Marcus, J. Arbiol, K. A. Moler, and P. Krogstrup, Semiconductor–ferromagnetic insulator–superconductor nanowires: Stray field and exchange field, Nano Lett. **20**, 456 (2020).
[32] S. Vaitiekėnas, Y. Liu, P. Krogstrup, and C. M. Marcus, Zero-bias peaks at zero magnetic field in ferromagnetic hybrid nanowires, Nat. Phys. **17**, 43 (2021).
[33] Y. Tserkovnyak, A. Brataas, and G. E. W. Bauer, Enhanced Gilbert Damping in Thin Ferromagnetic Films, Phys. Rev. Lett. **88**, 117601 (2002).
[34] A. Brataas, Y. Tserkovnyak, G. E. W. Bauer, and B. I. Halperin, Spin battery operated by ferromagnetic resonance, Phys. Rev. B **66**, 060404(R) (2002).
[35] Y. Tserkovnyak, A. Brataas, G. E. W. Bauer, and B. I. Halperin, Nonlocal magnetization dynamics in ferromagnetic heterostructures, Rev. Mod. Phys. **77**, 1375 (2005).
[36] A. Hirohata, K. Yamada, Y. Nakatani, I.-L. Prejbeanu, B. Diény, P. Pirro, and B. Hillebrands, Review on spintronics: Principles and device applications, J. Magn. Magn. Mater. **509**, 166711 (2020).
[37] J. Sinova, S. O. Valenzuela, J. Wunderlich, C. H. Back, and T. Jungwirth, Spin Hall effects, Rev. Mod. Phys. **87**, 1213 (2015).
[38] A. Hoffmann and S. D. Bader, Opportunities at the Frontiers of Spintronics, Phys. Rev. Appl. **4**, 047001 (2015).
[39] X.-L. Qi, T. L. Hughes, and S.-C. Zhang, Fractional charge and quantized current in the quantum spin Hall state, Nat. Phys. **4**, 273 (2008).
[40] D. Meidan, T. Micklitz, and P. W. Brouwer, Optimal topological spin pump, Phys. Rev. B **82**, 161303(R) (2010).
[41] D. Meidan, T. Micklitz, and P. W. Brouwer, Topological classification of interaction-driven spin pumps, Phys. Rev. B **84**, 075325 (2011).
[42] F. Mahfouzi, B. K. Nikolić, S.-H. Chen, and C.-R. Chang, Microwave-driven ferromagnet–topological-insulator heterostructures: The prospect for giant spin battery effect and quantized charge pump devices, Phys. Rev. B **82**, 195440 (2010).
[43] V. F. Becerra, M. Trif, and T. Hyart, Topological charge, spin, and heat transistor, Phys. Rev. B **103**, 205410 (2021).
[44] D. J. Thouless, Quantization of particle transport, Phys. Rev. B **27**, 6083 (1983).
[45] T. Ojanen, Magnetoelectric Effects in Superconducting Nanowires with Rashba Spin-Orbit Coupling, Phys. Rev. Lett. **109**, 226804 (2012).
[46] A. Y. Kitaev, Unpaired Majorana fermions in quantum wires, Phys. Usp. **44**, 131 (2001).
[47] See Supplemental Material at http://link.aps.org/supplemental/10.1103/PhysRevLett.130.237002 for more details on the dependence of the conductance and spin pumping with other barrier widths, the reflection coefficients, the fractional entropy, quasi-MZMs, robustness against disorder of the main results, and the magnetization dynamics, which includes Refs. [48–52].
[48] N. Hartman, C. Olsen, S. Lüscher, M. Samani, S. Fallahi, G. C. Gardner, M. Manfra, and J. Folk, Direct entropy measurement in a mesoscopic quantum system, Nat. Phys. **14**, 1083 (2018).

[49] T. Child, O. Sheekey, S. Lüscher, S. Fallahi, G. C. Gardner, M. Manfra, A. Mitchell, E. Sela, Y. Kleeorin, Y. Meir, and J. Folk, Entropy Measurement of a Strongly Coupled Quantum Dot, Phys. Rev. Lett. **129**, 227702 (2022).

[50] Y. Kleeorin, H. Thierschmann, H. Buhmann, A. Georges, L. W. Molenkamp, and Y. Meir, How to measure the entropy of a mesoscopic system via thermoelectric transport, Nat. Commun. **10**, 5801 (2019).

[51] C. Han, Z. Iftikhar, Y. Kleeorin, A. Anthore, F. Pierre, Y. Meir, A. K. Mitchell, and E. Sela, Fractional Entropy of Multichannel Kondo Systems from Conductance-Charge Relations, Phys. Rev. Lett. **128**, 146803 (2022).

[52] T. Child, O. Sheekey, S. Lüscher, S. Fallahi, G. C. Gardner, M. Manfra, and J. Folk, A robust protocol for entropy measurement in mesoscopic circuits, Entropy **24**, 417 (2022).

[53] M. V. Moskalets, *Scattering Matrix Approach to Non-Stationary Quantum Transport* (World Scientific, London, 2012).

[54] M. Blaauboer, Charge pumping in mesoscopic systems coupled to a superconducting lead, Phys. Rev. B **65**, 235318 (2002).

[55] C. W. Groth, M. Wimmer, A. R. Akhmerov, and X. Waintal, Kwant: A software package for quantum transport, New J. Phys. **16**, 063065 (2014).

[56] I. C. Fulga, B. van Heck, M. Burrello, and T. Hyart, Effects of disorder on Coulomb-assisted braiding of Majorana zero modes, Phys. Rev. B **88**, 155435 (2013).

[57] C. Mahaux and H. A. Weidenmüller, *Shell-Model Approach to Nuclear Reactions* (North-Holland, Amsterdam, 1969).

[58] J. Nilsson, A. R. Akhmerov, and C. W. J. Beenakker, Splitting of a Cooper Pair by a Pair of Majorana Bound States, Phys. Rev. Lett. **101**, 120403 (2008).

[59] H. Schomerus, Random matrix approaches to open quantum systems, arXiv:1610.05816.

[60] C.-X. Liu, F. Setiawan, J. D. Sau, and S. Das Sarma, Phenomenology of the soft gap, zero-bias peak, and zero-mode splitting in ideal Majorana nanowires, Phys. Rev. B **96**, 054520 (2017).

[61] S. O. Valenzuela and M. Tinkham, Direct electronic measurement of the spin Hall effect, Nature (London) **442**, 176 (2006).

[62] C. Brüne, A. Roth, H. Buhmann, E. M. Hankiewicz, L. W. Molenkamp, J. Maciejko, X.-L. Qi, and S.-C. Zhang, Spin polarization of the quantum spin Hall edge states, Nat. Phys. **8**, 485 (2012).